Memorias del 2022 Congreso Nacional de Control Automático
12-14 de Octubre, 2022. Tuxtla Gutiérrez, México.

Development of a 6-DOF robot for haptic interaction with complex virtual environments

Brayan Alonso-Torres * **José Daniel Castro-Díaz** **
Mauro López-Rodríguez * **Marco Arteaga** *

* *Departamento de Control y Robótica, División de Ingeniería Eléctrica, Facultad de Ingeniería, UNAM, Ciudad de México 04510, México. (e-mail: brayanalonso@comunidad.unam.mx, maurogbto@gmail.com, marteagp@unam.mx)*
** *Centro Tecnológico Aragón, Facultad de Estudios Superiores Aragón, UNAM, Estado de México 57130, México. (e-mail: josecastrocad@aragon.unam.mx)*

Abstract: In the last decade, the design and implementation of robots have taken a turnaround in areas such as haptics and virtual reality. Unlike the big and heavy industrial robots, haptic ones must be light and suitable to be easily handled by an operator. Moreover, they must have enough actuators to allow a realistic haptic interaction with complex virtual environments. In this work, we present the two phases Research and Development process of a six-degrees-of-freedom haptic robot. In the first phase, we build on our previous work to design a spherical wrist, improving both the mechanics and electronics of an old one. In the second phase, we design a virtual environment consisting of a ball and beam system with which the operator interacts visually and haptically. The basis of our development is the well-known Novint Falcon parallel robot that acts as the first 3-DOF of the resulting device. The rest is completed with an improved spherical wrist, in which a 6-DOF force sensor that measures the interaction forces between the virtual environment and the operator was mounted. Our ultimate goal is to evaluate the usability of the obtained haptic robot and present it as a viable alternative to current commercial devices.

Keywords: Parallel robot, spherical wrist, six degrees of freedom, virtual reality environment, haptic interaction.

1. INTRODUCTION

Interaction with virtual reality environments has taken an increasing interest in recent years by the scientific community. From videogaming to surgical simulation, this new area of development represents a disruption in science and technology. The basis of such interaction is a correct human senses stimulation and how close it is to reality. In this regard, the most used interaction channel is visual since it is easy to stimulate the sense of sight with the currently available display devices, e.g., a computer screen or an Oculus Rift headset. On the other hand, the sense of touch needs to be stimulated by more complex devices, capable of exerting a wide range of forces. That is where haptic robots play a major role.

The more complex the interfaces used to interact haptically with a virtual environment, the more realistic the interaction would be. In the case of haptic robots, this complexity lies in the number of degree-of-freedom and their capacity to render forces in six dimensions (Salisbury et al., 2004). Nevertheless, the most widely used haptic robots today have 6-DOF but only the first three of them are actuated. Such is the case of the Geomagic Touch device, a serial robot capable of reproducing forces but not torques in the Cartesian space. This is a disadvantage when the forces to be rendered come from complex virtual environments. For example, in surgery simulators, the operator needs to sense the reaction forces when starting to introduce a tool in a virtual tissue, but also when this tool is twisted once inside. A robot with only 3-DOF actuated will never be capable of rendering such forces.

The fastest option is to use a 6-DOF robot already available on the market, such as the sigma.7 robot by Force Dimension. Nevertheless, its high cost makes it unaffordable for most research groups that must not only direct their efforts to haptic developments, but also to other areas of robotics. The solution to this dilemma is to design robots from scratch Nguyen et al. (1991) or build on what others have developed, but adding their own innovations. From this perspective, the Novint Falcon parallel robot was used to develop the 6-DOF robot presented in this paper since its performance for virtual reality tasks has been tested previously (Rodríguez and Velázquez, 2012).

Even though it originally emerged as an accessory for video games, in recent years the Novint Falcon robot has been used as a research and development device in haptics for virtual reality (Scalona et al., 2017). In contrast with the Geomagic Touch, the Falcon has a parallel structure that

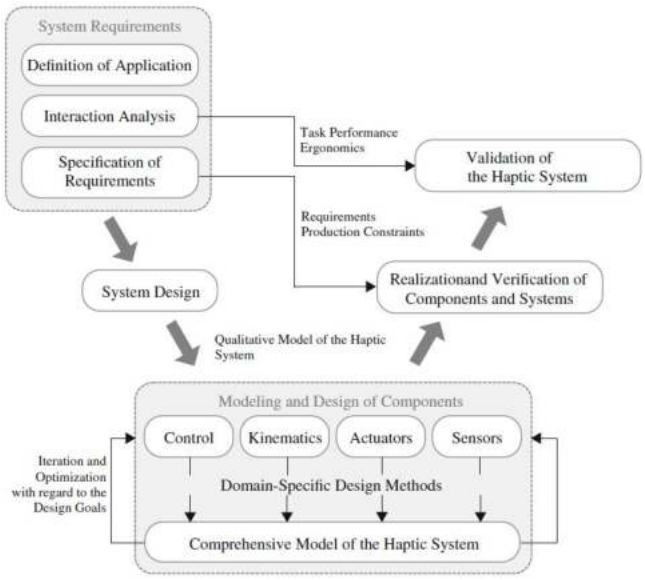

Fig. 1. V-model for haptic systems design

allows it to exert a greater range of forces. This is an advantage since a tool or a mechanism with considerable weight can be attached to its end-effector. For the second case, it is natural to think that such a mechanism could be an actuated spherical wrist if we want a haptic rendering that includes both forces and torques in the Cartesian space.

Adapting an spherical wrist to an already built robot requires the combined knowledge of specialists such as mechanical engineers, sensor and instrumentation professionals, software developers, and control engineers (Hatzfeld and Kern, 2009). Consequently, a haptic system developer should have multidisciplinary training, in addition to some basic notions of psychophysics and neurobiology. The result of this combination is the obtaining of devices that can be used in different applications as teleoperation (Jorda et al., 2022) or medical simulation for surgical training (Tobergte et al., 2011).

The integration of all the knowledge mentioned above is possible through design methods as the V-model for software development but adapted to mechatronic systems (Nattermann and Anderl, 2013), as can be seen in Figure 1. The core of the process is the stage of Modeling and Design of Components, where kinematics, control and selection of actuators and sensors play a major role. Once accomplished such a stage, it is necessary to integrate it with others and carry out iterations in order to find the correct system configuration.

In this paper we present a brief description of the implementation process for an fully-actuated 6-DOF robot composed by a Novint Falcon and a original designed spherical wrist mechanism. Following the V-model for haptic systems, we show a previous design iteration, identifying the necessary improvements for interaction with virtual environments. We test the performance of the device integrating it into a virtual reality ball and beam game and measuring the exerted forces by a 6-DOF force sensor.

The paper is organized as follows: the mathematical preliminaries for the kinematic design of the spherical wrist are given in Section 2. Section 3 presents the improvements with respect a previous design iteration. A experimental evaluation is presented in Section 4 and finally, some concluding remarks are given in Section 5.

2. PRELIMINARIES

The foundational problems that arise when studying and designing robots are forward and inverse kinematics. For the former, the homogeneous transformation matrix that relates the reference frame O_n with the reference frame O_0 is calculated as

$$^0\boldsymbol{T}_n(q_1, q_2, \ldots, q_n) = {}^0\boldsymbol{A}_1 {}^1\boldsymbol{A}_2 \ldots {}^{n-1}\boldsymbol{A}_n, \tag{1}$$

where $^{i-1}\boldsymbol{A}_i$ for $i = 1, 2, \ldots, n$ represents the position and orientation of two consecutive reference frames, established according the Denavit-Hartenberg convention.

For the inverse kinematics, it is necessary to find the solutions $q_1, q_2, \ldots, q_n$ of the equation

$$^0\boldsymbol{T}_n(q_1, q_2, \ldots, q_n) = \boldsymbol{T}_\mathrm{d}, \tag{2}$$

where $\boldsymbol{T}_\mathrm{d}$ represents the desired position and orientation of the end-effector (Spong et al., 2006).

2.1 Kinematic decoupling

For a 6-DOF robot, the common practice is to decouple the inverse kinematic problem into two simpler problems: inverse position kinematics and inverse orientation kinematics. In simpler words, the first three joints are used to modify the position of the end effector and the rest to modify its orientation. We can express equation (2) as

$$^0\boldsymbol{o}_6(q_1, q_2, \ldots, q_6) = \boldsymbol{o}_\mathrm{d} \tag{3}$$

$$^0\boldsymbol{R}_6(q_1, q_2, \ldots, q_6) = \boldsymbol{R}_\mathrm{d}, \tag{4}$$

where $\boldsymbol{o}_\mathrm{d}$ and $\boldsymbol{R}_\mathrm{d}$ are the desired position and orientation of the end-effector respectively.

Using equations (3) and (4) implies that the axes z_3, z_4, and z_5 intersect at a point O_c called the *spherical wrist center* and, therefore, the origins of the reference frames O_4 and O_5 will always be at such point (Spong et al., 2006). In practice, a spherical wrist has only revolute joints and is mounted on a 3-DOF robot. It is important to remark that the motion of the final three links about their axes will not change the position of O_c, therefore, the position of the wrist center is a function of only the first three joint variables (Siciliano et al., 2010).

2.2 Differential kinematics

The velocity relationships between joints are determined by the Jacobian of the forward kinematics and is expressed as

$$\boldsymbol{J}(\boldsymbol{q}) = \begin{bmatrix} \boldsymbol{J}_v(\boldsymbol{q}) \\ \boldsymbol{J}_\omega(\boldsymbol{q}) \end{bmatrix} = \begin{bmatrix} \boldsymbol{J}_{v_1}, \cdots, \boldsymbol{J}_{v_n} \\ \boldsymbol{J}_{\omega_1}, \cdots, \boldsymbol{J}_{\omega_n} \end{bmatrix}, \tag{5}$$

where $\boldsymbol{J}_v \in \mathbb{R}^{3\times n}$ expresses linear velocities and $\boldsymbol{J}_\omega \in \mathbb{R}^{3\times n}$ angular velocities.

Equation (5) allows to relate joint velocities with the velocities in the Cartesian space as

$$\dot{\boldsymbol{x}} = \boldsymbol{J}(\boldsymbol{q})\dot{\boldsymbol{q}}, \tag{6}$$

On the other hand, the forces can be mapped in the joint space as

$$\boldsymbol{\tau} = \boldsymbol{J}(\boldsymbol{q})^{\mathrm{T}}\boldsymbol{F}, \tag{7}$$

where $\boldsymbol{F} \in \mathbb{R}^{3\times 1}$ is the vector of forces in the Cartesian space.

Equations (6) and (7) are used only for serial manipulators. Since the Novint Falcon parallel robot plays as the first three joints of the 6-DOF robot, the mapping of velocities is obtained by

$$\dot{\boldsymbol{q}} = \boldsymbol{J}(\boldsymbol{q})\dot{\boldsymbol{x}}, \tag{8}$$

while the mapping of forces

$$\boldsymbol{F} = \boldsymbol{J}(\boldsymbol{q})\boldsymbol{\tau}. \tag{9}$$

The complete kinematic analysis and design of the Novint Falcon, can be found in (Stamper, 1997).

3. IMPLEMENTATION

Martínez-Fernández et al. (2018) presented a first prototype that included the Novint Falcon Robot and a spherical wrist, made with three Namiki 22CL-3501PG motors with an 80:1 reduction gearbox. Nevertheless, for haptic rendering purposes, such a reduction decreases the immersion degree of the virtual reality applications. Furthermore, the data acquisition/generation was performed through the microcontroller Arduino Due and the processing on a desktop PC.

A prototype based on the work mentioned above is shown in Figure 2. This arrangement allowed the kinematic decoupling between the Novint Falcon robot and the spherical wrist because the three rotation axes of the latter intersect at O_c. Moreover, this point is separated a distance $O_{\mathrm{EF_{NF}}}$ of the Novint Falcon's end-effector. As a result, the 6-DOF robot can be divided in two subsystems:

- Subsystem 1 – Three DOF: θ_1, θ_2 and θ_3 of the Novint Falcon, being its end-effector the center of the spherical wrist O_c and its base reference frame the point O_{NF} (Torres-Rodríguez et al., 2017).
- Subsystem 2 – Three DOF: θ_4, θ_5 and θ_6 of the spherical wrist. Its end-effector is O_{EF} and its base reference frame the point O_c.

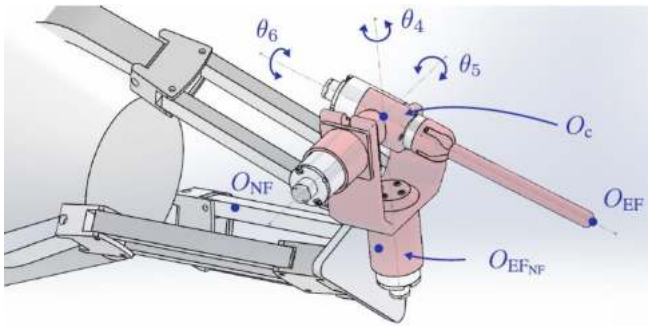

Fig. 2. Prototype based on (Martínez-Fernández et al., 2018)

The kinematic decoupling simplified the analysis, however, a problem arose when mapping the forces from the virtual environment. Since the 6-DOF robot obtained is a combination of a serial robot with a parallel one, it is not clear which of the equations (7) or (9) must to be used. The change of position of the Novint Falcon's end-effector moves O_c with respect to O_{NF}, but not its orientation, hence, the first three joints produce only linear velocity. On the other hand, when moving the reference frame O_{EF}, *i.e.*, the end-effector of the 6-DOF robot changes both position and orientation with respect O_c. This implies that the spherical wrist produces linear and angular velocity simultaneously, therefore, the equation (5) changes as

$$\boldsymbol{J}(\boldsymbol{q}) = \begin{bmatrix}\boldsymbol{J}_v(\boldsymbol{q}) \\ \boldsymbol{J}_\omega(\boldsymbol{q})\end{bmatrix} = \begin{bmatrix}\boldsymbol{J}_{\mathrm{NF}}(\boldsymbol{q}) & \boldsymbol{J}_{\mathrm{SW}_v}(\boldsymbol{q}) \\ \boldsymbol{0} & \boldsymbol{J}_{\mathrm{SW}_\omega}(\boldsymbol{q})\end{bmatrix} \tag{10}$$

where $\boldsymbol{J}_{\mathrm{NF}}(\boldsymbol{q}) \in \mathbb{R}^{3\times 3}$ is the Jacobian of the Novint Falcon [1], $\boldsymbol{J}_{\mathrm{SW}_v}(\boldsymbol{q}) \in \mathbb{R}^{3\times 3}$ is the Jacobian of the spherical wrist for linear velocities, $\boldsymbol{J}_{\mathrm{SW}_\omega}(\boldsymbol{q}) \in \mathbb{R}^{3\times 3}$ is the Jacobian for angular velocities and $\boldsymbol{0} \in \mathbb{R}^{3\times 3}$. Then, if equation (10) holds, both mechanisms remain coupled and the equations (7) and (9) cannot be used for haptic rendering.

3.1 Kynematic Design

The solution to the problem mentioned above consists of completely decoupling the rotational and translational space by making O_c and O_{EF} a same point. Therefore, the equation (10) is modified as

$$\boldsymbol{J}(\boldsymbol{q}) = \begin{bmatrix}\boldsymbol{J}_v(\boldsymbol{q}) \\ \boldsymbol{J}_\omega(\boldsymbol{q})\end{bmatrix} = \begin{bmatrix}\boldsymbol{J}_{\mathrm{NF}}(\boldsymbol{q}) & \boldsymbol{0} \\ \boldsymbol{0} & \boldsymbol{J}_{\mathrm{SW}_\omega}(\boldsymbol{q})\end{bmatrix}. \tag{11}$$

A kinematic chain that makes the equation (11) hold is shown in Figure 3, being the Sigma.7 robot from Force Dimension its inspiration. The joints were placed on the periphery of the spherical wrist in such a way its end-effector and its center shared the same point.

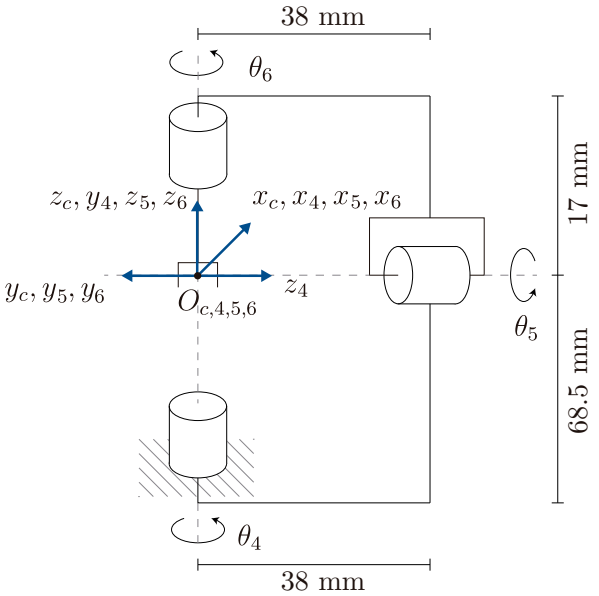

Fig. 3. Reference frames using the DH convention

The Denavit-Hartenberg parameters of the mechanism are shown in Table 1, being the difference with common spherical wrist arrangements that $d_6 = 0$.

[1] The equation of this Jacobian can be found in the work of Torres-Rodríguez et al. (2017).

Link	a_i [mm]	d_i [mm]	α [°]	θ [°]
4	0	0	90	θ_4
5	0	0	−90	θ_5
6	0	0	0	θ_6

Table 1. Denavit-Hartenberg parameters

Then, the corresponding homogeneous transformation matrices are

$$ {}^{c}\boldsymbol{A}_4 = \begin{bmatrix} \cos\theta_4 & 0 & \sin\theta_4 & 0 \\ \sin\theta_4 & 0 & -\cos\theta_4 & 0 \\ 0 & 1 & 0 & 0 \\ 0 & 0 & 0 & 1 \end{bmatrix} \tag{12} $$

$$ {}^{4}\boldsymbol{A}_5 = \begin{bmatrix} \cos\theta_5 & 0 & -\sin\theta_5 & 0 \\ \sin\theta_5 & 0 & \cos\theta_5 & 0 \\ 0 & -1 & 0 & 0 \\ 0 & 0 & 0 & 1 \end{bmatrix} \tag{13} $$

$$ {}^{5}\boldsymbol{A}_6 = \begin{bmatrix} \cos\theta_6 & -\sin\theta_6 & 0 & 0 \\ \sin\theta_6 & \cos\theta_6 & 0 & 0 \\ 0 & 0 & 1 & 0 \\ 0 & 0 & 0 & 1 \end{bmatrix}. \tag{14} $$

When multiplying equations (12), (13) and (14) according equation (1), the homogeneus transformation matrix ${}^{c}\boldsymbol{T}_6$ with respect to the reference system O_c is obtained. However, it does not match the position of the end effector of the Novint Falcon. For this reason, the matrix

$$ {}^{\mathrm{F}}\boldsymbol{A}_{\mathrm{c}} = \begin{bmatrix} 1 & 0 & 0 & p_x \\ 0 & 0 & 1 & p_y \\ 0 & -1 & 1 & p_z + of_z \\ 0 & 0 & 0 & 1 \end{bmatrix} \tag{15} $$

is used and where p_x, p_y and p_z represent the position of the Novint Falcon's end effector and of_z is an offset in the z axis direction. Therefore, the forward kinematics of the spherical wrist is

$$ {}^{F}\boldsymbol{T}_6 = \begin{bmatrix} c_4c_5c_6 - s_4s_6 & -c_6s_4 - c_4c_5s_6 & -c_4s_5 & p_x \\ c_6s_6 & -s_5s_6 & c_5 & p_y \\ -c_4s_6 - c_5c_6s_4 & c_5s_4s_6 - c_4c_6 & s_4s_5 & pz + \mathrm{ofz} \\ 0 & 0 & 0 & 1 \end{bmatrix} \tag{16} $$

where $c_i = \cos\theta_i$ and $s_i = \sin\theta_i$ for $i = 4, 5, 6$.

Finally, from the equation (16), the Jacobian of the 6-DOF robot can be obtained by substituting

$$ \boldsymbol{J}_{\mathrm{SW}_\omega}(\boldsymbol{q}) = \begin{bmatrix} 0 & \sin\theta_4 & -\cos\theta_4\sin\theta_5 \\ 1 & 0 & \cos\theta_5 \\ 0 & \cos\theta_4 & \sin\theta_4\sin\theta_5 \end{bmatrix} \tag{17} $$

in equation (11).

In Figure (4) the final prototype of the robot can be observed.

4. EXPERIMENTAL RESULTS

The 6-DOF robot developed is shown in Figure 5. While the Novint Falcon robot has already its own data acquisition/generation system, that of the spherical wrist was carried out through the controller Compact RIO 9014 and three NI-9505 H-bridge motor drive modules, one for each DOF. Moreover, since the perception of the forces during the interaction with the virtual environment is subjective, a 6-DOF force sensor ATI-Nano 17 was mounted at the

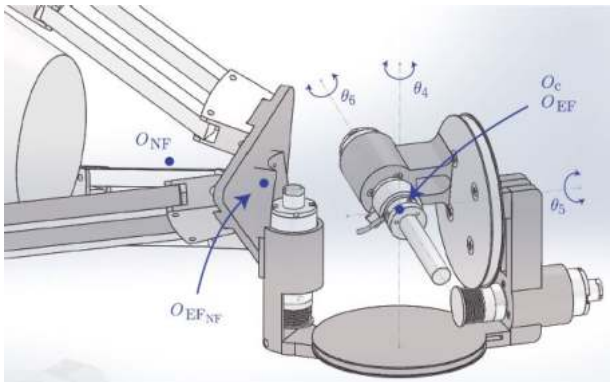

Fig. 4. Spherical wrist mounted on the Novint Falcon

end effector of the robot. This allows us to register the interaction forces and analyse their behavior objectively.

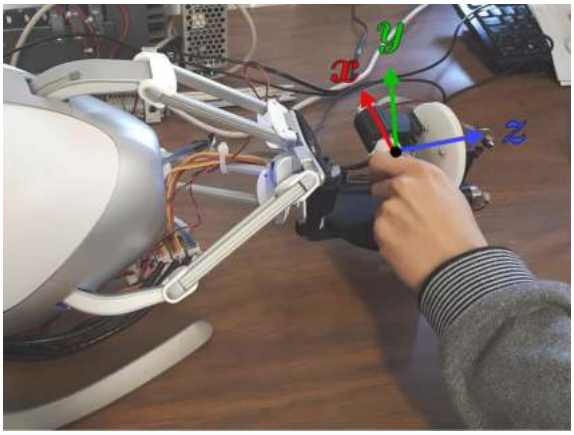

Fig. 5. 6-DOF robot obtained

4.1 Virtual environment

Complex environments consist of those where the operator can perceive objects of various shapes, both visually and haptically. In our case, we design an environment composed of a four walls room that the operator can walk through and a ball and beam game in the center. Such a game consists of a swinging plane where a sphere moves according to the movement of the plane produced by gravity. The goal is to avoid the ball falling onto the floor depending on the operator's movements. Naturally, neither the gravity nor the forces acting on the ball exist, therefore, it is necessary to simulate their physics and project it into the computer screen.

In Figure 6 a diagram of the ball and game at certain instant can be seen. The torque exerted by the sphere into the plane center is

$$ \boldsymbol{\tau}_{\mathrm{v}} = \boldsymbol{p} \times \boldsymbol{F} \tag{18} $$

where the sub-index v indicates that the torque is virtual, $\boldsymbol{p}$ is the position of the sphere and $\boldsymbol{F}$ the force due to the gravity.

The vector $\boldsymbol{p}$ is defined as

$$ \boldsymbol{p} = p_x\hat{i} \pm d\hat{j} + p_z\hat{k}, \tag{19} $$

where d is the distance between the XZ plane and the sphere, that depends on its position (negative or positive) on the y axis. The force exerted on the plane is

$$\boldsymbol{F} = -mg\hat{j}, \tag{20}$$

where m is the mass of the sphere, and g the constant of gravity.

Substituting (19) and (20) in (18) we obtain

$$\boldsymbol{\tau}_{\mathrm{v}} = p_z mg\hat{i} - p_x mg\hat{k} \tag{21}$$

and where is no torque exerted in y component.

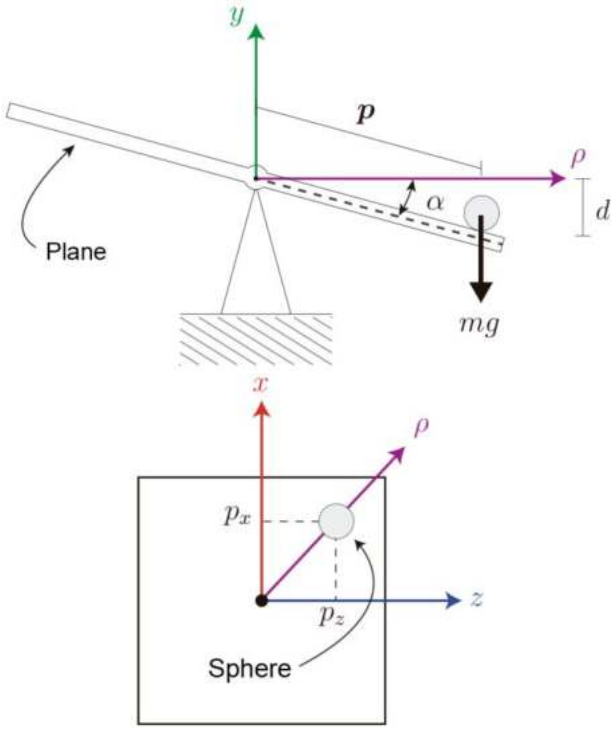

Fig. 6. Ball and beam system

The visual engine used for the virtual environment implementation was Unity, where the Jacobian of the spherical wrist maps the forces from the Cartesian space and it is not necessary to simulate any additional physical parameter of the behavior of the sphere. The result can be seen in Figure 7.

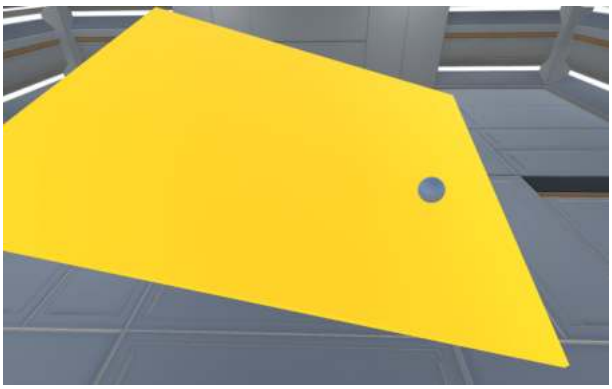

Fig. 7. Virtual environment rendered in Unity

Since in the Cartesian space there is not a force component in the y axis, once mapped the forces into the joint space, there is not response produced in q_4, *i.e.*, $\tau_{q_4} = 0$ as can be seen in Figure 8. Nevertheless, the force sensor registers the force produced by the operator sustaining the mechanism. On the other hand, the forces produced by the fifth and sixth joints are not equal to zero and they are shown in Figures 9 and 10 respectively. The curves present a mirroring effect since the forces are opposite according to Newton's second law. While the robot reproduces the forces of the virtual environment towards the operator, the force sensor registers those the operator exerts on the spherical wrist.

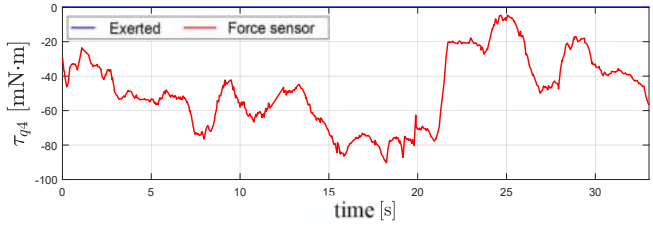

Fig. 8. Torque produced by joint q_4

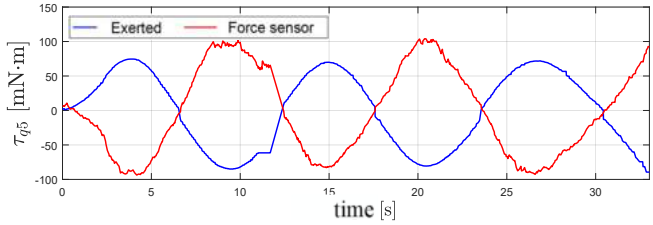

Fig. 9. Torque produced by joint q_5

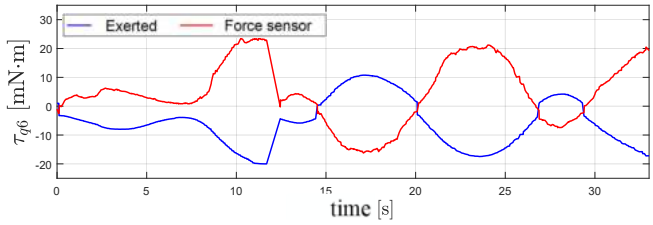

Fig. 10. Torque produced by joint q_6

It is important to remark that the apparent oscillatory behavior shown in Figures 9 and 10 is due precisely to the operator's attempts to balance the ball and try to take it to the center of the plane.

5. CONCLUSIONS

In this paper, we presented the development of a 6-DOF robot for haptic applications. We used the kinematic decoupling principle to design its spherical wrist while the Novint Falcon took the function of its first three degrees of freedom. The resulting device is an alternative to the expensive 6-DOF haptic robots on the market and was built taking into consideration the iterative V-model for haptic systems design. To test its performance, the robot was included in an application where the operator can perceive forces from a virtual environment where a ball and beam system was simulated. Through a 6-DOF sensor, we found that the force signals correspond to those produced in the virtual environment and felt by the operator.

In future work, we intend to carry out another iteration of the V-model, focusing on the kinematics of a parallel robot to replace the Novint Falcon. The goal is to obtain an original design for both mechanics and electronics of

the 6-DOF robot, identifying the possible innovations in haptics.

ACKNOWLEDGMENT

This work has been supported by the **DGAPA-UNAM** under grant **IN117820**.

REFERENCES

Hatzfeld, C. and Kern, T.A. (2009). *Engineering Haptic Devices: A beginner's guide*. Springer.

Jorda, M., Vulliez, M., and Khatib, O. (2022). Local autonomy-based haptic-robot interaction with dual-proxy model. *IEEE Transactions on Robotics*, 1–19. doi: 10.1109/TRO.2022.3160053.

Martínez-Fernández, E., Castro-Díaz, J.D., and Arteaga-Pérez, M.A. (2018). A spherical wrist prototype for the development of haptics applications with the Novint Falcon robot. *Memorias del Congreso Nacional de Control Automático 2018*, 335–340.

Nattermann, R. and Anderl, R. (2013). The W-Model – Using Systems Engineering for Adaptronics. *Procedia Computer Science*, 16, 937–946. doi: https://doi.org/10.1016/j.procs.2013.01.098. 2013 Conference on Systems Engineering Research.

Nguyen, C., Antrazi, S., Zhou, Z.L., and Campbell, C.E. (1991). Analysis and implementation of a 6 DOF Stewart platform-based robotic wrist. *Computer Electric Engineering*, 17, 191–203.

Rodríguez, J.L. and Velázquez, R. (2012). Haptic Rendering of Virtual Shapes with the Novint Falcon. *Procedia Technology*, 3, 132–138. doi: https://doi.org/10.1016/j.protcy.2012.03.014.

Salisbury, K., Conti, F., and Barbagli, F. (2004). Haptic Rendering: Introductory Concepts. *IEEE Computer Graphics and Applications*, 14, 24–32.

Scalona, E., Hayes, D., Palermo, E., Del Prete, Z., and Rossi, S. (2017). Performance evaluation of 3D reaching tasks using a low-cost haptic device and virtual reality. In *2017 IEEE International Symposium on Haptic, Audio and Visual Environments and Games (HAVE)*, 1–5. doi:10.1109/HAVE.2017.8240350.

Siciliano, B., Sciavicco, L., Villani, L., and Oriolo, G. (2010). *Robotics Modelling, Planning and Control*. Springer Verlag.

Spong, M.W., Hutchinson, S., and Vidyasagar, M. (2006). *Robot modeling and control*, volume 3. Wiley New York.

Stamper, R.E. (1997). *A Three Deggre of Freedom Parallel Manipulator with Only Translational Degree of Freedom*. Ph.D. thesis, University of Maryland. URL `https://drum.lib.umd.edu/handle/1903/5902`.

Tobergte, A., Helmer, P., Hagn, U., Rouiller, P., Thielmann, S., Grange, S., Albu-Schäffer, A., Conti, F., and Hirzinger, G. (2011). The sigma.7 haptic interface for mirosurge: A new bi-manual surgical console. In *2011 IEEE/RSJ International Conference on Intelligent Robots and Systems*, 3023–3030. doi: 10.1109/IROS.2011.6094433.

Torres-Rodríguez, I., Castro-Díaz, J.D., and Pliego-Jiménez, J. (2017). The Novint Falcon parallel robot as experimental haptic platform (El robot paralelo Novint Falcon como plataforma experimental háptica). *Memorias del Congreso Nacional de Control Automático 2017*, 587–593.